JOURNAL OF MATERIALS SCIENCE: MATERIALS IN MEDICINE **13** (2002) 495–500

Electrochemical and microstructural studies of tantalum and its oxide films for biomedical applications in endovascular surgery

R. A. SILVA
CIEA/ISEP, Rua S. Tomé, 4200 Porto, Portugal and INEB, Rua Campo Alegre, 823, 4150 Porto, Portugal

M. WALLS, B. RONDOT, M. DA CUNHA BELO
CECM/CNRS, 15 rue Georges Urbain, 94407 Vitry-sur-Seine Cedex, France

R. GUIDOIN
IBQ, 10, rue de l'Espinay, Québec (Québec) G1L 3L5, Canada

The most popular coronary stents are made of 316L stainless steel and self-expandable Nitinol. Nevertheless, Ta has already been used to make stents for endovascular surgery and may constitute a good alternative to the other materials because of its higher corrosion resistance and radio-opacity property, which may facilitate the follow-up of stent catheterization. The characterization of Ta and its natural passive oxide films has been performed in a 0.15 M NaCl solution (simulated body fluid – SBF) using anodic polarizations, electrochemical impedance spectroscopy and photoelectrochemical techniques. Changes in microstructure have been observed by atomic force microscopy (AFM). Polarization curves show the existence of a current density increase between 1.40 and 1.80 V. Bode complex plots show that some perturbation of the film occurred in this potential interval which may be associated with a decrease in polarization resistance, Rp, indicating that the film may be less resistant to corrosive attack. Mott–Schottky capacity measurements show that the density of donors, Nd, varies with polarization. The optical band gap, E_g, which is equal to 4.1 eV did not show variations in our experiments. The localized formation on the electrode surface, in the above potential interval of a Ta compound (possibly an oxide-hydroxide) was observed by AFM, and this may explain the appearance of the current density peak and capacity behavior at those potentials.
© *2002 Kluwer Academic Publishers*

1. Introduction

Coronary stents have acquired recently a great popularity in cardiovascular surgery. Since the first human implantation of a coronary stent by Sigwart *et al*. in 1986 [1] important progress has been made in this matter, mainly due to the persistent works of some researchers. Some studies concerning the implantation of the most widely used and best known stent, the Palmaz–Schatz stent [2–4] have been performed. Today in the literature, fortunately, the amount of published work on coronary stent implantation is substantial [5–18]. The stents are mainly made of stainless steel and Nitinol. A few tantalum stents have also been used [9–11]. In previous work we have seen that Ta is the most corrosion resistant material [19] is radio-opaque and biocompatible [20–24]. For these reasons, Ta may constitute a good alternative to stainless steel and Nitinol. Nevertheless, an abnormal current density increase with a maximum value occurring at around 1.65 V is always present when performing anodic polarizations of tantalum electrodes in our solution, this is why we decided to carry out more detailed research on Ta and its natural passivation films. Passive films constitute the first barrier against corrosion. The breakdown of these films leads to corrosion phenomena, associated with an increase in current density, as has been observed, with release of metallic ions to the adjacent tissues. These thin oxide films have semiconducting properties [25, 26]. The aim of this work was to characterize the natural oxide films in a simulated body fluid using impedance and photoelectrochemical spectroscopies as well as atomic force microscopy for the observation *in situ* of morphological and possible chemical surface changes during anodic polarizations.

2. Materials and methods

Disks of pure Tantalum (Ta $>$ 99.9% – Goodfellow) of 15 mm diameter and 5 mm thickness have been used in this work.

Prior to testing, the electrodes were cleaned in an ultrasonic bath with 1,1,1, trichloroethane, ethanol and bipermuted water. After this the samples were rapidly introduced into the cell containing 0.15 M NaCl solution.

Polarization curves were obtained 1 h after immersion in the solution, varying the potential between − 0.5 and 2.5 V, with a sweep rate of 0.25 mV/s. The current density was measured using a EG&G 273A potentiostat. A saturated calomel electrode (SCE) was used as the reference electrode and a platinum wire served as auxiliary electrode. Bode complex plots were obtained varying the frequency between 100 kHz and 50 mHz 1 h after immersion in the solution for open circuit potential, 0.95, 1.65 and 2.45 V. Mott–Schottky impedance spectroscopy were performed imposing a 10 kHz frequency to the electrode, which was immersed in the solution for 1 h before testing, with the aid of a EG&G 5208 lock-in analyzer and varying the potential between − 0.25 V (open-circuit potential) and − 2.5 V. Samples have also been polarized up to 2.45 V in the same conditions, to form a thicker film on which capacity measurements were performed down to − 2.5 V.

Photoelectrochemical experiments were carried out using the same potentiostat and lock-in amplifier coupled to ORIEL optical facilities with a xenon XBO 150 W lamp as a source of radiation and a 1200/mm grating monochromator (Jobin Yvon H25). The photocurrents were obtained by focusing the light with a fused silica lens trough a quartz window in the electrochemical cell onto the working electrode. The separation of the photocurrents from the passive film current was achieved by chopping the light at a frequency of 19 Hz and tuning the lock-in amplifier to select this frequency component in the current output from the potentiostat.

A Topometrix 2010 ''Discoverer'' atomic force microscope (AFM) was used to obtain images in real time while performing anodic polarizations between 0 and 3 V. The AFM apparatus was working in contact mode, with a liquid cell and silicon tips. After degreasing the samples with ''teepol'' and rinsing with bipermuted water in an ultrasonic bath, the samples were transferred to the cell which was filled with the 0.15 M NaCl solution. The scan speeds were of the order of 100 μm/s and the force used was as low as possible (∼ 1 nN).

3. Results and discussion

3.1. Anodic polarizations

In Fig. 1 is shown one of the anodic polarization curves. As one can see, there is a current density increase with maximum value at around 1.65 V followed by a decrease. One explanation for this electrochemical behavior is as follows: some localized dissolution of Ta associated with breakdown of the film occurs, corresponding to the increase in current density followed by a decrease in current density associated with repair of the film and its repassivation. We shall see that according to photoelectrochemical results, this phenomenon appears under the influence of an applied voltage which corresponds to the energy of the bandgap and can be related to the transition from semiconducting to dielectric behavior.

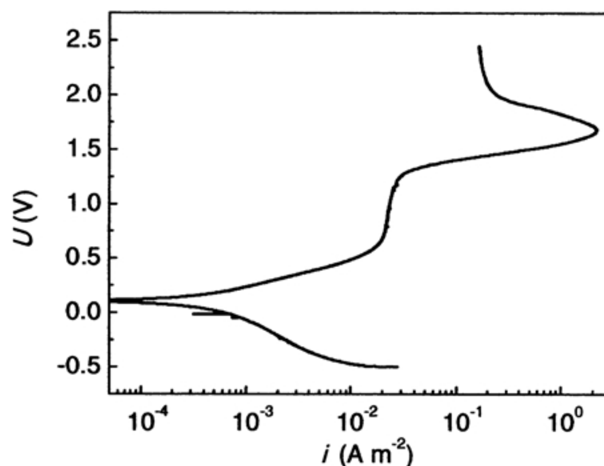

Figure 1 Anodic polarization curve of tantalum.

3.2. Impedance spectroscopy

Fig. 2 shows the Bode complex plots and in Table I are given the results of these experiments. As one can see for applied potential of 1.65 V some perturbation of the film occurs, followed by a decrease in its calculated polarization resistance as shown in Table I. These results show that a probable corrosion process occurs for these experimental conditions, confirming the results of the anodic polarization curves. Fig. 3 represents the variation of C^{-2} with potential for the film/electrolyte interfaces, with an applied frequency of 10 kHz. In this curve some distinct regions of the film's behavior are shown. In region 1 the capacity value is very high and independent of the polarization, the film is in electrical charge accumulation and allows current flow. In region 2 the capacity value decreases as a function of applied potential; this behavior corresponds to the depletion of donors and to the formation of a space charge layer (typical Mott–Schottky behavior) and the film shows a semiconducting character. In region 3 the capacity is again independent of applied potential; the donors are completely depleted and do not contribute to the capacity measurement. Our system is equivalent to a single capacitor. In region 4 the evolution of capacity values follows a similar C^{-2} vs. U law. This variation may indicate that for potentials above 0.6 V (potential at pH = 7 of the reaction $2H_2O = O_2 + 4H^+ + 4e^-$) film growth occurs and a space charge layer again exists of thickness W, thinner than the thickness of the film in formation. The 5th region corresponds to a potential interval in which the film growth is perturbed and the C^{-2} vs. U law is not followed – this potential interval corresponds to that in which abnormal behavior of the film was observed in the polarization curves and the Bode impedance measurements. In the 6th region the film grows and this is detectable by the changing color of the electrodes.

In order to propose a model for the electronic structure of the films we need to know several parameters: flat band potential U_{fb}, donor concentration N_d, and gap energy E_g. At open circuit potential our experiments have shown that the very thin oxide film (∼ 2 nm) formed on Ta exhibits a Mott–Schottky behavior for potentials varying between − 2 and − 0.5 V. The passivation film capacity is controlled by the space charge layer created at

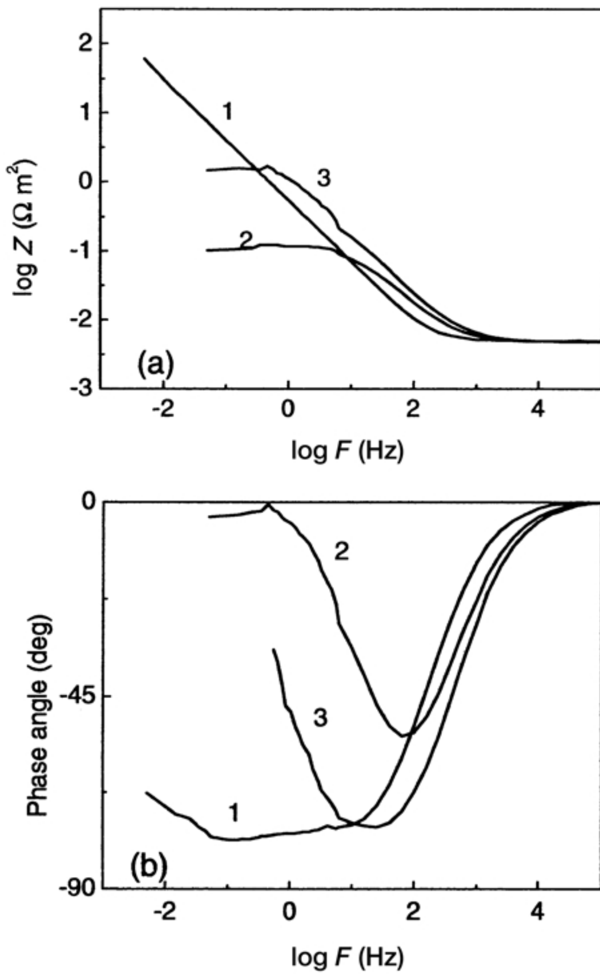

Figure 2 Bode complex plots of tantalum under different applied potentials (a) magnitude, (b) phase, 1 – open circuit potential, 2 – 1.65 V, 3 – 2.45 V.

the film/electrolyte interface as a function of the applied potential and gives rise to a positive straight line indicating that we have an *n*-type semiconducting behavior. The capacity is then represented by the Mott–Schottky equation:

$$\frac{1}{C_2} = \frac{2}{\varepsilon\varepsilon_0 e N_d}\left(U - U_{fb} - \frac{kT}{e}\right) \qquad (1)$$

where ε_0 is the permittivity of free space, ε is the dielectric constant of the semiconductor, N_d is the donor concentration and U_{fb} is the flat-band potential. In our case N_d is equal to 1.3×10^{27} at./m^3 with $\varepsilon = 18.5$ [27] and $U_{fb} = -2.1$ V.

This equation applies to an ideal Mott–Schottky junction. The potential drop produced by a polarization has its effect on the space charge layer. This means that the capacity of this layer is much smaller than the

TABLE I Results of Bode impedance measurements

$U(V)$	$R_s(\Omega\,\mathrm{m}^2)$	$R_p(\Omega\,\mathrm{m}^2)$
OCP	3.5	66.000
0.4	3.5	19.500
0.9	4.5	9.700
1.65	3.4	0.125
2.45	3.4	1.582

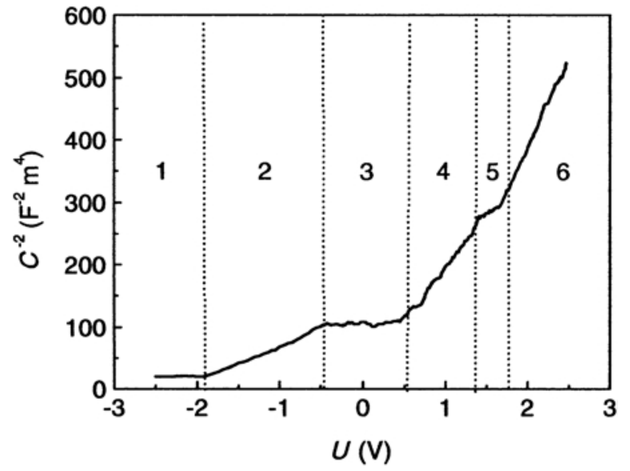

Figure 3 $C^{-2} = f(U)$ behavior of Ta in different regions of applied potential.

capacity of the Helmoltz layer. On the other hand, both the dielectric constant and the donor concentration of the semiconductor must have low values. This is not the situation in our case and so the Mott–Schottky Equation (1) must be rewritten as follows:

$$\frac{1}{C_2} = \frac{1}{C_H^2} + \frac{2}{\varepsilon\varepsilon_0 e N_d}\left(U - U_{fb} - \frac{kT}{e}\right) \qquad (2)$$

The capacity of the Helmoltz layer is taken as equal to $0.25\,\mathrm{F}\cdot\mathrm{m}^2$ [25]. We have then to take into account this capacity and use the equation of R. De Gryse [28]:

$$\frac{1}{C_{sc}^2} = \frac{1}{C^2} - \frac{1}{C_H^2} \qquad (3)$$

This relation does not change the linearity of the Mott–Schottky curve, there will just be a shift for more positive values of the flat band potential, which in our case will be equal to -1.85 V (Fig. 4).

The thickness of the space charge layer, *W*, may be calculated using the equation:

$$C = \frac{\varepsilon\varepsilon_0}{W} \qquad (4)$$

and depends equally on the difference between applied potential and flat band potential $(U - U_{\mathrm{fb}})$

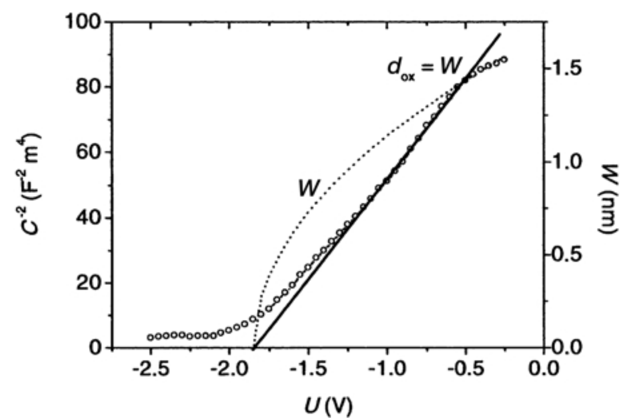

Figure 4 C^{-2} and *W* (thickness of space charge layer) as functions of applied potential.

TABLE II Results of Mott–Schottky measurements

$U(V)$	$U_{fb}(V)$	Donors (at. m^{-3})
OCP	− 1.82	1.3×10^{27}
2.45	− 2.00	2.3×10^{26}

$$W=\left[\frac{2\varepsilon\varepsilon_0}{eN_d}\right]^{1/2}\left[U-U_{fb}-\frac{kT}{e}\right]^{1/2} \quad (5)$$

In Fig. 4 is shown the influence of the potential on the thickness of the space charge layer and on the capacity, and in Table II the results of capacity measurements for films at − 0.25 (OCP) and 2.45 V. As one can see, the U_{fb} and N_d values are lower for the film formed at 2.45 V. In particular, the lower value of N_d must be associated with film thickening. On the other hand it seems that the Mott–Schottky equation is not respected for applied potentials equal to or higher than that for which the thickness of the space charge layer is identical to the estimated thickness of the oxide film.

4. Photoelectrochemical spectroscopy

For this study we used the Gartner model for metal–semiconductor interfaces [29] modified by Butler [30] and Ginley [31] for semiconductor–electrolyte interfaces. According to these authors, the photocurrent intensity I_{ph} may be calculated using the following equation:

$$I_{ph}=-e\Phi_0\left(1-\frac{e^{-\alpha_\lambda\cdot w}}{1+\alpha_\lambda L_p}\right) \quad (6)$$

where e is the electronic charge, Φ_0 is the photon flux, α_λ is the adsorption coefficient at wavelength λ, and L_p the diffusion length.

At constant potential (thickness of space charge layer, W, constant) and variable wavelength the photocurrent is solely controlled by absorption which is characterized by the coefficient α_λ. Nevertheless the variation law of α_λ as a function of the energy, $h\nu$, is not simple and depends on selection rules which control the electronic transition probabilities. In the case of an amorphous semiconductor, the photocurrent variation as a function of the energy, $h\nu$, may be expressed as follows:

$$h\nu\cdot I_{ph}=-e\Phi_0 WA(h\nu-E_g)^n \quad (7)$$

where A is a constant and the value $n=2$ (the most commonly adopted value) corresponds to indirect transitions.

Using this equation, one can calculate the energy of the forbidden band, E_g, through the straight line $[(I_{ph}/e\Phi)h\nu]^{0.5}$ as a function of the energy, $h\nu$, where $(I_{ph}/e\phi)$ is the quantum efficiency η (Fig. 5). E_g is found to be equal to 4.1 eV, which is in accordance with other literature data [32].

5. Atomic force microscopy (AFM)

Fig. 6 shows AFM *in situ* images of the tantalum surface at different stages of the anodic polarization. All images were acquired from essentially the same 10 × 10 μm

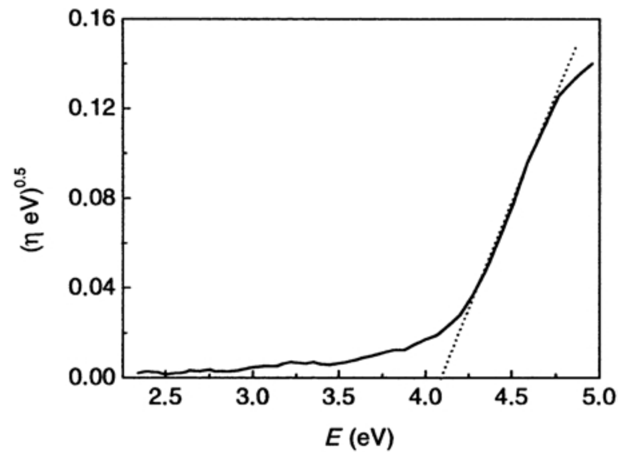

Figure 5 Determination of E_g for an indirect transition (tantalum).

region, although there was a small amount of drift during the lengthy experiment. The almost vertical lines visible in all the images are polishing scratches. No significant change is visible for applied potentials between 0 and 1.4 V. This implies that if any film growth takes place during this time it is extremely uniform. Between 1.4 and 1.8 V (the range corresponding to the peak in anodic current) the appearance of small localized growths is observed at what seem to be random points on the tantalum surface. In particular, no correlation has been observed between the local planarity or roughness of the surface and the probability of growth formation – they do not appear to be aligned along the scratch marks, for example. The growths range in size from about 10 to 100 nm, although the size of the smaller ones may be somewhat exaggerated in the images through convolution with the shape of the AFM tip, which has an end radius of the order of 10 nm. Further polarization from 1.7 up to 2.45 V produces little variation in the aspect of the surface. As to the nature of the growths themselves, we have little evidence currently available. Preliminary investigations using scanning and transmission electron microscopy indicate that they are probably amorphous and do not contain significant amounts of incorporated electrolyte species. These results will be presented in full elsewhere when complete. We think that these growths are likely to be composed of a tantalum oxide-hydroxide compound.

6. Band structure of the film

For the interpretation of the electron transfer reactions we need a picture of the electronic structure of the oxide film. The schematic band structure model is presented in Fig. 7. Because the oxide is an n-type semiconductor with very high doping density, the Fermi level is situated very close to the lower edge of the conduction band [25]. In addition, according to photoelectrochemical results the band gap energy is approximately 4 eV. If we consider that electronic equilibrium exists between the metal/film and film/solution interfaces, then, under the influence of an anodic potential the bands bend down and develop space charge regions (Schottky barriers) at each interface (Fig. 7(a))

It is important to note that the height of the barrier at

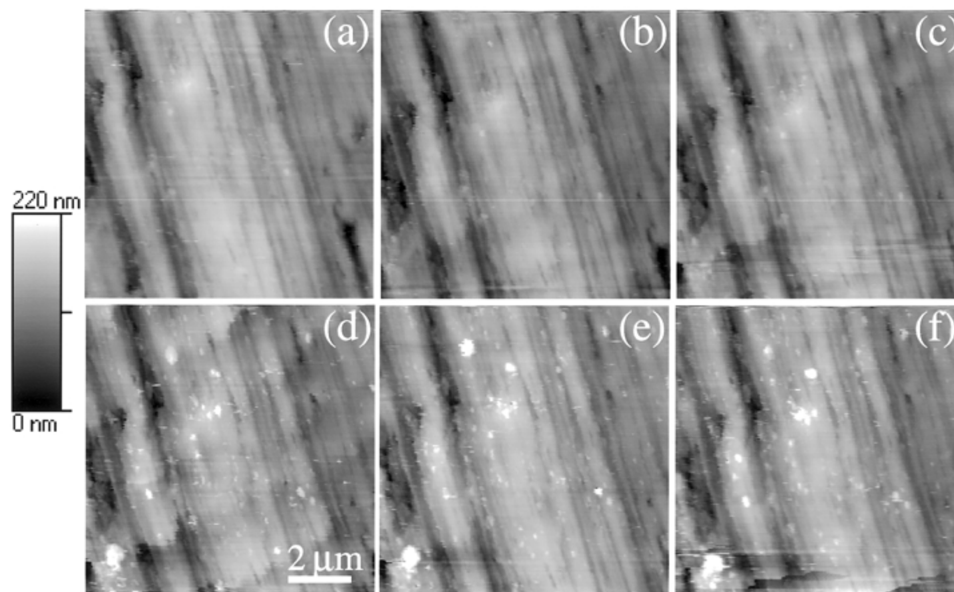

Figure 6 AFM images for different applied potentials, (a) open circuit potential, (b) 0.9 V, (c) 1.35 V, (d) 1.65 V, (e) 1.85 V, (f) 2.45 V.

both metal/film and film/solution interfaces also depends on the concentration of mobile ions [33]. In fact, the local field may not be strongly affected when the concentration of mobile ions is small, but for very high concentration the field strength decreases particularly close to the interfaces. In the case of films formed on tantalum, the point defects generated are cation and anion vacancies at the film/solution and metal/film interfaces respectively.

According to the capacitance results represented in Fig. 3 the film reveals first Mott–Schottky behavior (region 2). Then, in region 3 the thickness of the space charge layer is not potential dependent (the film is depleted). When the polarization potential reaches region 4 the decrease in capacitance observed may be related to the influence of oxygen evolution. It is also necessary to take into account the fact that under the influence of the applied potential the energy of the conduction band, in the bulk of the film, approaches that of the valence band. Under these conditions, by a dominant process similar to that which occurs in a tunnel junction, the electrons in the valence band can enter into the conduction band by tunnelling (Fig. 7(b)). Thus, the anodic current increases (peak) and promotes the very localized processes of film growth observed by AFM (Fig. 6) With increasing polarization, tunneling is not possible, we arrive at a situation in which the electronic band profile is no longer determined by the electronic distribution as in semiconductors but by the properties of the mobile ionic carriers, which become the majority carriers with increasing voltage. At this point the classical anodic process becomes operative (Fig. 7(c)).

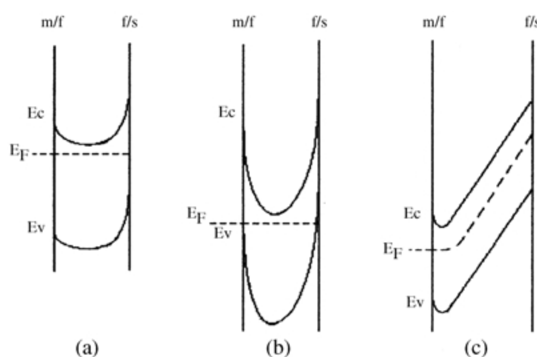

Figure 7 Band structure schematic model. Development of band bending downwards under applied anodic potential (a), tunneling of electrons into the conduction band (b), operative anodic ion process (c).

7. Conclusions

Polarization and Bode impedance experiments have shown that there exists a peculiar behavior of natural oxide films of tantalum between 1.4 and 1.8 V where the current density increases and polarization resistance decreases. This may indicate that localized corrosion followed by repassivation with film growth has occurred. The film growth was observed, *in situ*, by AFM. Mott–Schottky impedance studies show that tantalum films have semiconducting characteristics, the gap value being equal to 4.1 eV. The proposed band structure model associates the observed current peak to a situation of transition from semiconducting to dielectric behavior.

Acknowledgments

ICCTI/French Embassy in Portugal Convention, Project 107/B is gratefully acknowledged. The Calouste Gulbenkian Foundation is gratefully acknowledged. Research support funding from the IPP is gratefully acknowledged.

References

1. U. SIGWART, J. PUEL, V. MIRKOVITCH, F. JOFFRE and L. KAPPENBERGER, *New Engl. J. Med.* **316**(12) (1987) 701–706.
2. P. W. SERRUYS, P. DE JAEGERE, F. KIEMENEIJ, C. MACAYA, W. HEINDRICKX *et al*., *ibid.* **331**(8) (1994) 489–495.
3. D. L. FISCHMAN, M. B. LEON, D. S. BAIM, R. A. SCHATZ, M. P. SAVAGE, I. PENN *et al*., *ibid.* **331**(8) (1994) 496–501.
4. P. W. SERRUYS, H. EMANUELSSON, W. VAN DER GIESSEN, A. C. LUNN, F. KIEMENEY, C. MACAYA *et al*., *Circulation* **93**(3) (1996) 412–422.

5. D. J. COHEN, J. A. BREALL, K. K. HO, R. E. KUNTZ, L. GOLDMAN, D. S. BAIM *et al*., *ibid*. **92** (1995) 1859–1874.
6. D. J. COHEN, J. A. BREALL, K. K. HO, R. M. WEINTRAUB, R. E. KUNTZ, M. C. WEISTEIN *et al*., *J. Amer. Coll. Cardiology* **22**(4) (1993) 1052–1059.
7. D. J. COHEN, H. M. KRUMHOLZ, C. A. SUKIN, K. K. HO, R. B. SIEGRIST, M. CLEMAN *et al*., *Circulation* **92** (1995) 2480–2487.
8. A. COLOMBO, P. HALL, S. NAKAMURA, Y. ALMAGOR, L. MAIELLO, G. MARTINI *et al*., *ibid*. **91**(6) (1995) 1676–1688.
9. J. J. GOY, E. EECKHOUT, J. C. STAUFFER, P. VOGT and L. KAPPENBERGER, *Catheter. Cardiov. Diag*. **34** (1995) 128–132.
10. N. HAMASAKI, H. NOSAKA and M. NOBUYOSHI, *J. Amer. Coll. Cardiol*. **239A** (1995) (special issue).
11. C. W. HAMM, C. BEYTHIEN, H. SIEVERT and A. LANGER, *Amer. Heart J.* **129**(3) (1995) 423–429.
12. F. KIEMENEIJ, J. HOFLAND, G. J. LAARMAN, D. HUPKENS VAN DER ELST and H. VAN DER LUBBE, *Catheter. Cardiov. Diag*. **35** (1995) 301–308.
13. V. K. MEHAN, U. KAUFMANN, P. URBAN, P. CHATELAIN and B. MEIER, *ibid*. **34** (1995) 122–127.
14. N. M. ROBINSON, M. R. THOMAS, D. E. JEWITT and R. J. WAINWRIGHT, *Cardiology* **7**(6) (1995) 156–164.
15. J. C. STAUFFER, E. EECKHOUT, J. J. GOY, C. A. NACHT, P. VOGT and L. KAPPENBERGER, *J. Invas. Cardiol*. **7**(8) (1995) 221–227.
16. J. WEBB, S. STERTZER, T. AHMAD, R. CARERE, B. MERCIER and A. DODEK, *Catheter. Cardiov. Diag*. **37** (1996) 120–124.
17. A. A. SCHÖNEBERGER and K. SCHMIDT, *New Engl. J. Med.* **335**(15) (1996) 1160.
18. K. A. PRIESTLEY, J. R. CLAGUE, N. P. BULLER and U. SIGWART, *Europ. Heart J.* **17**(3) (1996) 438–444.
19. R. A. SILVA, M. A. MARQUES, A. SILVEIRA, M. WALLS, B. RONDOT and R. GUIDOIN, in ''Proceedings of the 14th European Conference on Biomaterials, The Hague, September 1998'', edited by the Dutch Society for Biomaterials, p. 37.
20. C. M. J. M. PYPEN, H. PLENK JR, M. F. EBEL, R. SVAGERA and J. VERENISCH, *J. Mater. Sci. Mater. Med.* **8** (1997) 781–784.
21. J. B. PARK, in ''Biomaterials Science and Engineering'' (New York, Plenum Press, 1984) p. 217.
22. P. F. JONHSON, J. J. BERNSTEIN, G. HUNTER, W. W. DAWSON and L. L. HENCH, *J. Biomed. Mater. Res.* **11** (1977) 637–656.
23. J. BLACK, *Clin. Mater.* **16** (1994) 167–173.
24. G. J. STACKPOOL, A. B. KAY, P. MORTON, E. J. HARVEY, M. TANZER and J. D. BONE, in ''Proceedings of Combined Orthopaedic Research Societies Meeting'', edited by Orthopaedic Research Society (Rider Dickerson Inc., Chicago, 1995) p. 45.
25. V. A. MACAGNO and J. W. SCHULTZE, *J. Electroanal. Chem.* **180** (1984) 157–170.
26. J. W. SCHULTZE and V. A. MACAGNO, *Electrochim. Acta* **31** (1986) 355–363.
27. O. KERREC, D. DEVILLIERS, H. GROULT and M. CHEMLA *Electrochim. Acta* **40** (1995) 719–724.
28. R. DEGRYSE, W. P. GOMES, F. CARDON and J. VENNIK *J. Electrochem. Soc.* **122** (1975) 711.
29. W. W. GARTNER, *Phys. Rev.* **116** (1959) 84.
30. M. A. BUTLER, *J. Appl. Phys.* **48** (1977) 1914.
31. D. S. GINLEY and M. A. BUTLER, *ibid*. **48** (1977) 2019.
32. P. CLECHET, J-R. MARTIN, R. OLIER and C. VALLOUY, *C. R. Acad. Sci. Paris* **282** (1976) 887–890.
33. M. M. LOHRENGEL, *Electrochim. Acta* **39** (1994) 1265–1271.

Received 31 August 2000
and accepted 23 October 2001